Hindawi
Journal of Nanomaterials
Volume 2022, Article ID 9980031, 9 pages
https://doi.org/10.1155/2022/9980031

Research Article

Probing the Thermal Behavior and Stability of Metal-Fe_3O_4 Heterodimer Nanoparticles Utilizing *In Situ* Pulsed Laser Heating TEM

Garrett M. Mitchell,[1] Shoumya Nandy Shuvo,[2] Subhajit Kundu,[3] Michael J. Manto,[4] Chao Wang,[4] and Volkan Ortalan[5]

[1]*Davidson School of Chemical Engineering, Purdue University, West Lafayette, Indiana 47907, USA*
[2]*School of Materials Engineering, Purdue University, West Lafayette, Indiana 47906, USA*
[3]*Department of Chemical Engineering and Materials Science, University of Minnesota, 421 Washington Ave. SE, Minneapolis, MN 55455, USA*
[4]*Department of Chemical and Biomolecular Engineering, Johns Hopkins University, Baltimore, Maryland 21218, USA*
[5]*Department of Materials Science and Engineering, University of Connecticut, Storrs, Connecticut 06269, USA*

Correspondence should be addressed to Volkan Ortalan; vortalan@uconn.edu

Received 16 March 2021; Accepted 2 December 2021; Published 14 February 2022

Academic Editor: Lavinia Balan

In situ laser heating with transmission electron microscopy (ILH-TEM) is utilized as a neoteric method to probe the thermal behavior and stability of metal- (Pt, Au-) metal oxide (Fe_3O_4) heterodimer (HD) nanoparticles. Two different supporting membrane types are used for the laser heating: pure-carbon and silicon-nitride, requiring different amounts of laser power to induce morphological changes. Diffraction pattern analysis and scanning transmission electron microscopy (STEM) and electron energy loss spectroscopy (EELS) are utilized to analyze reduction of the iron oxide under laser heating, which has differing effects depending on the support film heating mode and the heterodimer particle. A unique wetting behavior of Pt and Au onto Fe_3O_4 is observed in both heterodimers of Au and Pt. However, this wetting behavior is found to be partially reversible only in the case of the Au-Fe_3O_4 HD system, whereas for the Pt-Fe_3O_4 HD system, this wetting process was found to be irreversible under the applied experimental conditions. This observation of a novel wetting behavior has future implications for understanding the performance of oxide supported metal nanoparticles in high temperature applications, such as catalysis.

1. Introduction

Metal nanoparticles supported on oxides have long been of paramount importance in catalysis for water purification, emission reduction in cars, the water-gas shift reaction and the methane/propane oxidation reaction [1–7]. In this regard, size and shape of the nanomaterials have been shown to play a crucial role in improving catalytic activity [8–10]. Reduction in size leads to higher activity per unit mass of the catalyst, but due to concomitant increase in surface free energy, there is a higher tendency to sinter. The high temperature and reactive conditions encountered during catalysis often accelerate the sintering process, which results in a loss of active surface area of the nanoparticles, causing an undesired catalyst deactivation. An unwanted shape change may further pose a threat to the activity. Apart from the shape/size, tuning the metal-support interaction (MSI) has been a key factor in improving functionality of catalytic systems [11]. Over the past two decades, there have been plenty of studies on the bonding between gold/platinum and metal oxide supports showing not only high catalytic activities [12, 13] but also high stability [14] against sintering. Often abrupt change in activity has been observed at higher temperature [15, 16]; therefore, studying the evolution of shape/size with temperature is important to correlate the high temperature catalytic activity with its respective shape/size.

To investigate this stability behavior, we employ a study involving the use of plasmonics, a growing field of nanotechnology where the interaction between the electromagnetic fields and the free electrons in metal nanostructures are being studied [17, 18]. Many exciting research directions have emerged by the virtue of the wide variety of chemical and physical processes that can be induced by light [19–22]. The advent of lasers provided a useful system to investigate and control plasmonic materials. Along with the development of the novel nanomaterial synthesis route called laser ablation [23, 24], the ability of laser pulses to heat locally in a controlled and efficient way also makes it promising for architecting nanomaterials with good precision. The synchronized use of electron microscopy and lasers resulted in the possibility of *in situ* laser heating transmission electron microscopy (ILH-TEM), which has enabled spatial and temporal studies of structural dynamics with nanoscale resolution [25–31]. Real-time data was achieved with ILH-TEM utilizing different electron microscopy techniques, such as real-space imaging, diffraction, and electron energy loss spectroscopy (EELS) [25, 26]. In order to further investigate samples after ILH-TEM imaging, scanning transmission electron microscopy (STEM) is used since it provides a unique advantage for imaging. Through the exploitation of high angle scattered electrons, detectible by a high angle annular dark field (HAADF) detector, which depends on strong atomic number (Z^2) contrast (incoherent imaging), direct interpretation of an image is possible. While HAADF-STEM imaging is very valuable in imaging localized nanoscale regions with Z-contrast, ILH-TEM imaging exploits the utilization of lasers which give rise to a profound way to study laser-matter interactions, such as a plasmonic study of nanomaterials. Therefore, utilization of both techniques offers the full potential of electron microscopy in providing direct images and precise characterization of local nanostructures in real-time to achieve a fundamental understanding of dynamic processes occurring in nanomaterials.

Here, we report the use of in situ laser heating experiments to probe the dynamic behavior and stability of Pt-Fe_3O_4 heterodimer (HD) and Au-Fe_3O_4 HD particles. The laser heating causes the Pt particles to undergo complete wetting onto Fe_3O_4, proving evidence for strong metal support bonding (MSB). A partial dewetting after cooling is observed in the Au-Fe_3O_4 HD system while no noticeable dewetting after cooling was observed for the Pt-Fe_3O_4 HD system, which could be understood by thermodynamic analysis. Understanding the nature of how these particles behave under heating gives insights into the precise control of the metal oxide supports in rational design of a stable metal catalyst.

2. Methods

In this experiment, two types of materials were used: Au-Fe_3O_4 HD and Pt-Fe_3O_4 HD with two different kinds of TEM support membranes, a copper grid with an amorphous carbon support membrane (referred to as carbon support membrane) and a silicon-nitride support membrane (Ted Pella, Inc.). Synthesis of Au-Fe_3O_4 HD and Pt-Fe_3O_4 HD nanoparticles was made possible by inaugurating the epitaxial growth of Fe on Au and Pt nanoparticles (NP) seeds followed by Fe oxidation in an organometallic solution synthesis [25–27]. The main objective of employing organic methods of synthesis was to ensure regulation of the nanoparticles and a controlled uniform growth of Fe_3O_4 on the exposed (111) facets of the Au and Pt seeds.

For both Au-Fe_3O_4 HD and Pt-Fe_3O_4 HD nanoparticles, the nanoparticles were dispersed in hexane (3-6 mg/mL) which was then further diluted with hexane in a separate container to avoid surplus of samples on the grid. The purpose of hexane was to prevent any agglomeration and clump formation of the nanoparticles when the sample is loaded on the grid.

Two drops of hexane mixed with the heterodimers were then drop casted on both the grid types before they were placed in the sample holder. *In situ* TEM images and videos were obtained by using a modified FEI Tecnai T20 200 kV. Samples were heated via pulsed frequency doubled Nd-YAG laser beam with a wavelength of 532 nm, pulse frequency of 25 kHz, a pulse duration of 1 ns, and $1/e^2$ spot size of ~80 μm. The laser was first set at a minimum power of 3 mW. After loading the holder with either grid containing HD nanoparticles (copper grid with an amorphous carbon membrane or a Si_3N_4 membrane) into the goniometer, the sample was irradiated with a laser excitation pulse starting from a minimum power of 3 mW, which then is gradually increased with a step size of 0.44 mW up until reaching to a power where the heterodimers show some structural or positional changes via TEM. The region of interest (ROI) was selected in such a way as to utilize effectively the Gaussian heating profile of the laser. The samples were also imaged for only 30 minutes for each ROI (much more than the time required to induce wetting under these laser heating conditions) to ensure that the structural changes in the HD nanoparticles were induced by laser heating and not by the electron radiation required for TEM imaging. No changes in the HD nanoparticles were observed via only electron radiation in this time scale.

SAED diffraction patterns were collected both before and after the laser irradiation. The corresponding patterns were then analyzed to index the spots to determine the materials or phases present in the sample.

HAADF-STEM images were collected at 300 kV on a FEI Titan ETEM 80-300 kV in an *ex situ* condition. STEM-EELS, as well as some of the HAADF-STEM imaging, was performed on a JEOL JEM-ARM200cF utilizing a GIF Quantum SE Imaging Filter operated in Dual-EELS mode in an *ex situ* condition as well. *Ex situ* scanning TEM (STEM) electron energy loss spectroscopy (EELS) was performed after the laser irradiation of the Au-Fe_3O_4 HD and Pt-Fe_3O_4 HD nanoparticles to probe "local" chemical nature of the nanoparticles through point scans and spectrum imaging.

Figure 1 displays the experimental set up of the ILH-TEM, which was utilized to study the laser-assisted annealing of the HD nanoparticles. The setup consisted of a specialized TEM with a port of entry for the laser beam and an optical bench, wherein the laser beam was generated

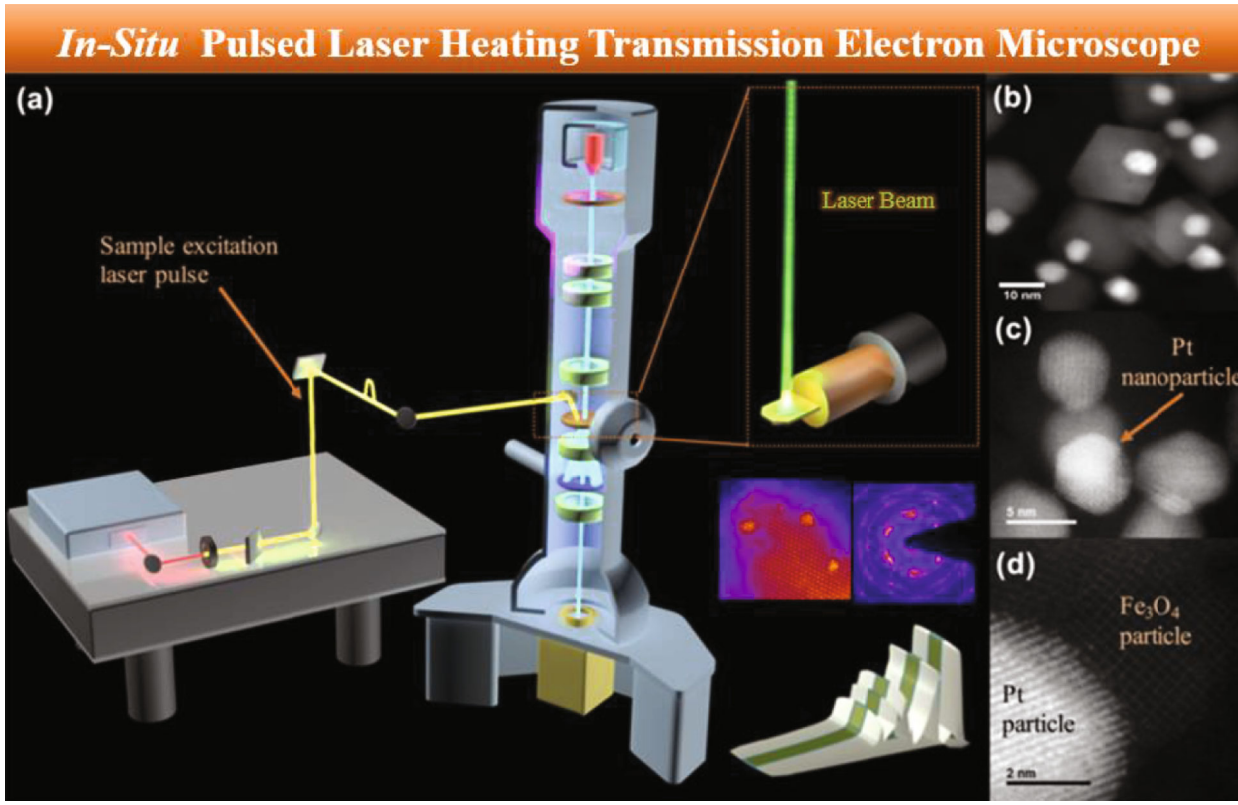

Figure 1: (a) Schematic diagram of the experimental set up of an in situ laser heating transmission electron microscope. (b) HAADF-STEM image of Pt HD system. (c, d) HR-STEM images of Pt and Fe_3O_4 nanoparticles at atomic resolution.

and processed before entry into the TEM. In regular operation of an ILH-TEM, a sample excitation laser is used to induce change in the sample. Herein, the sample excitation laser (532 nm Nd-YAG laser operating at 25 kHz with pulse duration of ~1 ns) along with continuous thermionic emission mode of the ILH-TEM is utilized to carry out the laser-assisted thermal annealing study on the HD nanoparticles. The HD nanoparticles were synthesized using a wet chemical route reported elsewhere [32–34]. Fe is grown epitaxially on (111) facets of Au or Pt nanoparticles and is subsequently oxidized to form the metal-Fe_3O_4 HDs. Figures 1(b)–1(d) show low magnification and atomic resolution HAADF-STEM images of a typical Pt-Fe_3O_4 HD nanoparticle sample. The spacing between the array of Pt atoms was precisely measured to be 2.2 Å, which corresponds to the (111) plane of Pt.

3. Results and Discussion

Figure 2(a) shows bright field- (BF-) TEM images of Pt-Fe_3O_4 HD nanoparticles supported on a carbon support membrane before laser irradiation. Laser irradiation of this region at a power of 7 mW (Figures 2(b)–2(e)) reveals that the Pt nanoparticles (NPs) spread and cover the Fe_3O_4 nanoparticles at higher temperatures, which would indicate wetting of the Fe_3O_4 NPs by the epitaxial Pt NPs. The relevant particles in Figure 2 are color coded for clarity. In addition, the HD particles are seen to undergo sintering (Supporting Movie-1). After completion of the laser irradiation process, there was negligible amount of dewetting of Pt from Fe_3O_4, indicating that such a transformation is irreversible under the experimental conditions. It can be noted that there is a cavity left by the sintering nanoparticles; this is seen for both the Si_3N_4 and the carbon film case (Figures 2(e) and 3(d)) and can be due to etching of the support by the nanoparticles. It can also be noted that there is some carbon contamination present in this system that could potentially affect the reduction process of Fe and even potentially form iron carbides [35]. However, carbon XPS studies in the literature show that there is no iron carbide formation under similar conditions [36], making the potential for iron carbide formation unlikely.

Similar experiments were carried out with Au-Fe_3O_4 HD nanoparticles, in which a laser power of 5 mW was needed to undergo transformation (Figures 2(h)–2(l)). We can estimate that the temperature for Au wetting is on the order of ~500°C by comparison with a previously published result [36]. Since the laser power required to induce the transformation for the Pt HD system is higher, temperatures in excess of 500°C would be expected for the Pt HD system. It is well known that for an Au film grown on single crystalline Fe_3O_4, the interfacial adhesion between the Au and Fe_3O_4 is weaker compared to the Au-Au bonding, shown by the formation of 3D island shapes, following a Volmer-Weber growth mode [37, 38]. Indeed, to create a 2D film of Au on (111) Fe_3O_4 via UHV sputtering, the Au film thickness must be as high as 7 nm, at temperatures below 200°C. Such 2D films, however, can be created with Pt with a film

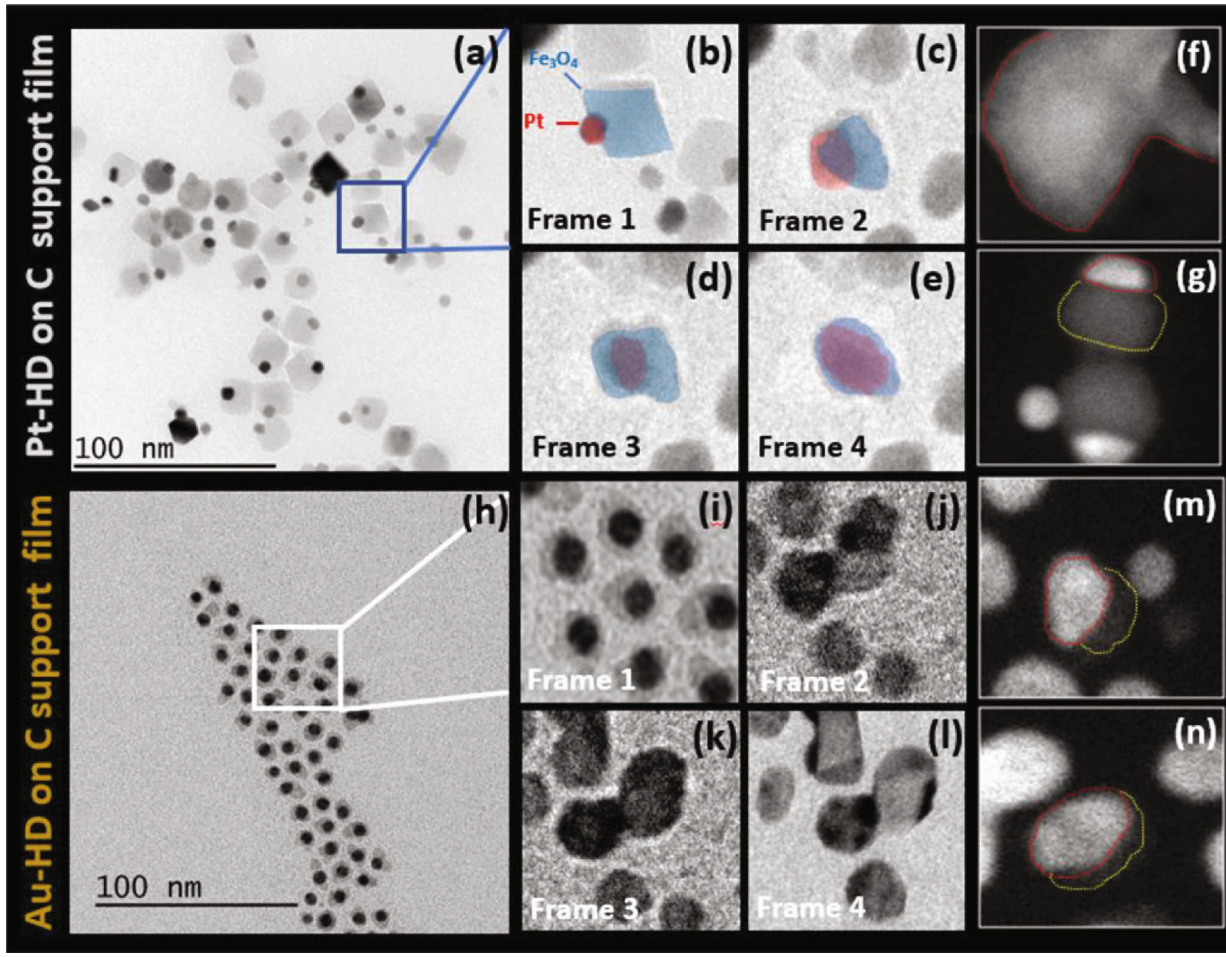

Figure 2: TEM micrographs displaying the heterodimer wetting behavior on a carbon support membrane (a, h) bright field- (BF-) TEM images of Pt and Au heterodimers, respectively, before laser irradiation. (b–e, i–l) Frames taken from the in situ laser heating TEM movie which illustrates the wetting process of the Pt and Au, respectively, onto the Fe_3O_4. (f, g, m, n) HAADF-STEM images of Pt and Au heterodimers, respectively, after laser irradiation.

thickness as low as 2 nm and are stable to a much higher temperature of 750°C [37, 38]. However, this effect is contrary to our results for the Au-Fe_3O_4 HD system: Au particles spread onto the Fe_3O_4, wetting the Fe_3O_4 NPs at higher temperatures above 200°C and lower film thickness than 7 nm. Also, unlike the Pt HD system, partial dewetting of Au from Fe_3O_4 was observed after the laser irradiation was stopped. To further investigate this result, HAADF-STEM images were acquired from different regions which clearly shows the partial dewetting of Au resulting in formation of two-faced Janus particles (Figures 2(m) and 2(n)). Some of the particles in TEM and STEM images are color coded for clarity.

The notable difference between the dewetting behavior of Au and Pt onto Fe_3O_4 could be due to the difference in the strength of the metal support bonding (MSB). An estimate of MSB strength under annealing conditions can be obtained using Young-Dupre equation:

$$E_{adh} = \gamma_{np}(1 - \cos\theta), \quad (1)$$

where θ is the contact angle and γ_{np} is the surface energy of the supported nanoparticle.

In both cases (Au and Pt), complete wetting of the surface of Fe_3O_4 is observed, making the contact angle, θ, equal to 180°. But, since the surface energy of (111) Pt (2.489 J/m^2) is higher than Au (1.506 J/m^2) by a factor of 1.65 [39, 40], the interfacial adhesion of Au is expected to be lower than Pt by a factor of 0.61. It can also be noted that Au has a lower melting point (1064°C or 1337 K) than Pt (1768°C or 2041 K) [41]. Pt is also known to form many different full alloys with Fe, while Au will only form dilute solid solutions, indicating that the Pt-Fe interfacial energy is lower, or more relevant than for the Au-Fe system, hence making the Pt-Fe wetting more stable [42, 43]. Therefore, surface energy and bulk phase diagrams support the experimental result that Au dewets from Fe_3O_4, while Pt does not.

Pt heterodimers were required to be exposed more laser power (7 mW) to show viable occurrence of visible dynamics than Au heterodimers (5 mW). The higher power requirement in Pt could be explained by two main effects: a difference in energy required to induce wetting and a difference in laser absorbance of the two HD systems. Although the HD

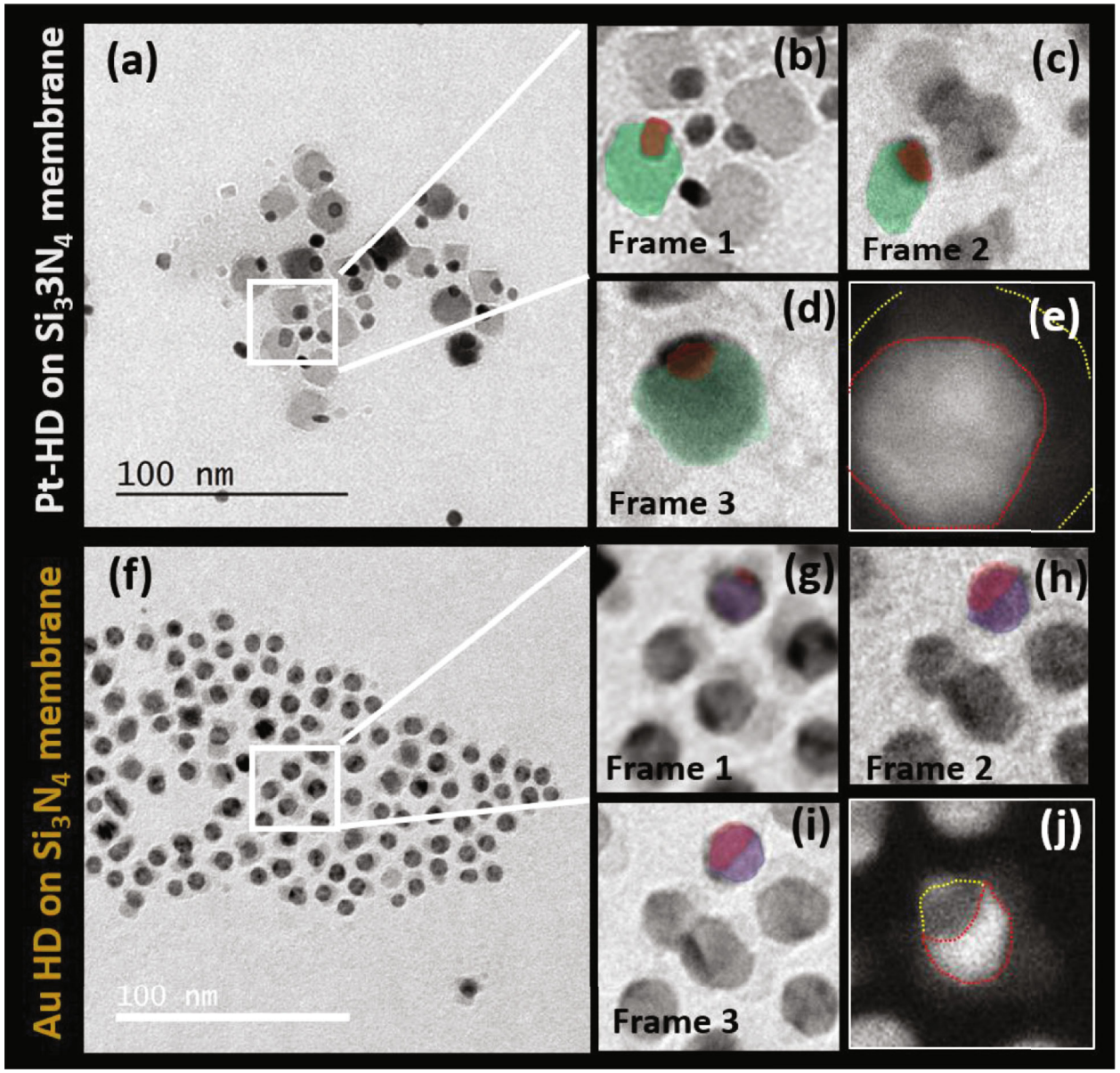

Figure 3: TEM micrographs displaying the heterodimer wetting behavior on a silicon nitride support membrane (a, f) bright field- (BF-) TEM images of Pt and Au heterodimers, respectively, before laser irradiation. (b–d, g–i) Frames taken from the *in situ* laser heating TEM movie which illustrates the wetting process of the Pt and Au, respectively, onto the Fe_3O_4. (e, j) HAADF-STEM images of Pt and Au heterodimers, respectively, after laser irradiation.

particles have complex nanostructures in which the exact surface energies are difficult to compute, the planar surface energy ratio of Pt and Au is 1.65 : 1 and is a rough model that can be used for a baseline, supporting the observed higher power requirements for the Pt system. Moreover, from the literature, the absorbance of Pt-Fe_3O_4 HD at 532 nm (the wavelength of the laser used in this experiment) is lower (~1.8x) than the absorbance of the Au-Fe_3O_4 HD nanoparticles [44, 45]. The reduced absorbance of the Pt heterodimer system paired with the Pt:Au planar surface energy ratio of 1.65 : 1 (similar to the absolute melting point ratio of 1.53 : 1) elucidates the higher power requirement of the Pt heterodimer system.

Figure 3 demonstrates the result for laser heating of the HD nanoparticles on the silicon nitride (Si_3N_4) support membrane. For both the Pt-Fe_3O_4 HD and Au-Fe_3O_4 HD systems, it was observed that the laser power required to visualize any possible dynamics (such as wetting) was lower for the carbon support membrane compared to the Si_3N_4 support membrane by a factor of 2.88 averaged over the two sample types. This laser power Si_3N_4/carbon is remarkably similar to the carbon/Si_3N_4 DRUV-VIS Kubelica-Munk function ratio of 2.68 (shown in Fig. S-1). This indicates that the laser heating mechanism for both of these support types is dominated by laser absorption of the support and not the nanoparticles themselves. This conclusion is further made

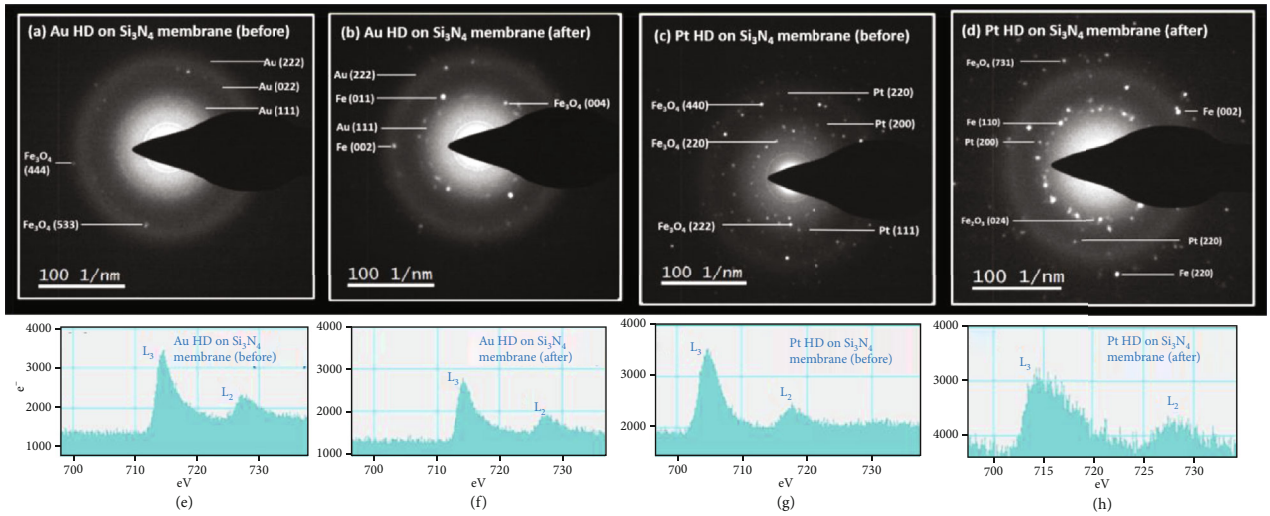

FIGURE 4: (a, b) SAED diffraction patterns of Au-Fe_3O_4 HD on a Si_3N_4 support membrane of a region of interest before and after laser irradiation, respectively. (c, d) SAED diffraction patterns of Pt-Fe_3O_4 HD on Si_3N_4 support membrane of a region of interest before and after laser irradiation, respectively. (e, f) EELS spectra showing Fe L_3 and L_2 edges before and after laser irradiation on Au-Fe_3O_4 HD on Si_3N_4 support membrane, respectively. (g, h) EELS spectra showing Fe L_3 and L_2 edges before and after laser irradiation on Pt-Fe_3O_4 HD on Si_3N_4 support membrane, respectively.

solid by the observation that the Pt/Au required laser power ratio on silicon nitride is 1.38, which is similar to the ratio on the carbon membrane. If laser heating was performed mainly by direct plasmonic heating of heterodimer nanoparticles, the required Pt/Au laser power ratio would be closer to 2.97 : 1 as indicated in the previous paragraph. Thus, laser heating on silicon nitride is also dominated by laser absorption of the support and not by the heterodimer nanoparticles.

To investigate any potential differences in chemistry between the two different support membranes, diffraction pattern analyses were carried out on both kinds (Pt-Fe_3O_4 HD and Au-Fe_3O_4 HD) of samples. Figures 4(c) and 4(d) and 5(c) and 5(d) show diffraction patterns of Pt heterodimers supported on the silicon nitride and carbon support membranes, respectively, before and after laser irradiation. The appearance of rings indicates the presence of multiple nanocrystals of the heterodimers inside the selected area diffraction (SAED) aperture. Indexing of the spots shows the presence of Pt and Fe_3O_4 crystal phases upon laser irradiation of Pt-Fe_3O_4 HD on both the silicon nitride and carbon support membrane. In this case, distinct diffraction spots corresponding to Fe were observed after laser irradiation indicating partial reduction of Fe_3O_4 to Fe after laser irradiation. This auto reduction behavior is well known in the literature and is known to be directly proportional to the temperature under vacuum [46]. A very similar result was observed for the case of Au-heterodimers which has been shown in Figures 4(a) and 4(b) and 5(a) and 5(b), wherein faint spots corresponding to Fe were observed along with that of Au and Fe_3O_4 in both the systems comprising Si_3N_4 and carbon support membrane grids, indicating partial reduction of Fe_3O_4 to Fe.

The reduction of Fe_3O_4 after laser treatment was further investigated using STEM-EELS. Figures 4(e)–4(h) show the EELS spectrum of the Pt-Fe_3O_4 HD and Au-Fe_3O_4 HD samples before and after laser irradiation on a Si_3N_4 support membrane. The peaks were identified using the EELS atlas, Fe L_3 edge being the more intense peak at ~715 eV, and Fe L_2 edge being the less intense peak at ~725 eV [47]. Since calculation of the oxidation state of Fe by the use of chemical shifts is not reliable when there are systems of mixed Fe oxidation states [48], the white-line intensity method was used to visualize the overall oxidation state. The peaks were first background subtracted using an inverse power law method, then deconvoluted by using the Fourier ratio method so that thickness effects were removed from the peak intensities. A double-atan function with a sharpness of 1 eV was fitted to the continuum, so that the continuum was subtracted from the white-line peaks [49]. The intensity of each peak was then measured with an energy window of 8 eV, and the resulting ratio of the L_3 intensity over the L_2 intensity was used to track the change in the average oxidation state of the Fe [50]. Reference peaks from HD nanoparticles before laser heating and from standard samples of Fe_2O_3 and metallic Fe (bulk form) were obtained for comparison to demonstrate that the white-line intensity ratio will reduce upon reduction. However, since these bulk structures do not have the same fine structure as the HD nanoparticles, their white-line intensity values cannot be directly compared to those in the HD systems. A tabulated form of the quantification data in Table 1 shows the white-line intensity ratios of Fe L_2 and L_3 edges of the reference samples of Fe and Fe_2O_3 and the HD before and after laser irradiation. It can be clearly seen that after laser treatment, the Pt-Fe_3O_4 HD system undergoes a more rigorous reduction as the white-line intensity ratio undergoes a larger percent change of 63% compared to the Au-Fe_3O_4 13% change in peak ratio, as well as having a higher percent difference from the initial

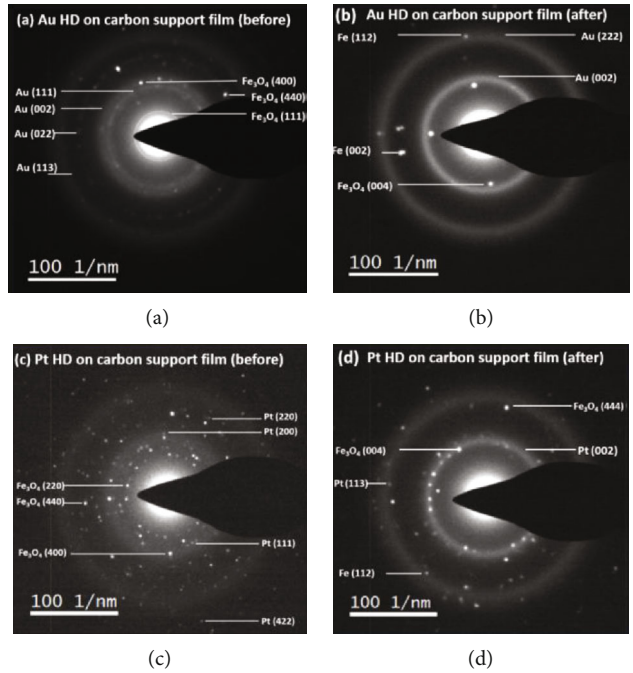

(a) (b) (c) (d)

Figure 5: (a, b) SAED diffraction patterns of Au-Fe_3O_4 HD on a carbon support membrane of a region of interest before and after laser irradiation, respectively. (c, d) SAED diffraction patterns of Pt-Fe_3O_4 HD on a carbon support membrane of a region of interest before and after laser irradiation, respectively.

Table 1: Tabulated values of the integral ratio of the Fe L_3 and L_2 edges of the heterodimers before and after laser irradiation with included Fe reference states.

Sample	Initial	Laser-treated	% difference
Fe_2O_3 ref.	4.36 ± 0.44	—	—
Fe ref.	3.18 ± 0.13	—	—
Pt-Fe_3O_4 HD on Si_3N_4 membrane	3.89 ± 0.33	2.03 ± 0.73	63.02%
Au-Fe_3O_4 HD on Si_3N_4 membrane	3.29 ± 0.39	2.89 ± 0.23	13.03%

HD white-line intensity peak ratio than the carbon support membrane. This behavior can partly be explained by the fact explanation for why the Au-Fe_3O_4 HD wetting is semireversible where the Pt-Fe_3O_4 HD wetting is not, fine-structure changes that would change the white-line intensity ratio. However, this difference in the amount of reduction is likely simply due to higher laser power and thus higher temperature, required to induce morphological changes in the Pt-Fe_3O_4 HD system.

4. Conclusions

In conclusion, we have probed the thermal behavior and stability of Pt-Fe_3O_4 HD and Au-Fe_3O_4 HD nanoparticles utilizing the in situ capabilities of an ILH-TEM. It was found that both Pt and Au nanoparticles undergo wetting onto Fe_3O_4, an indication of strong metal support bonding. *In situ* BF-TEM and SAED analyses, *ex situ* HAADF-STEM imaging, and STEM-EELS spectroscopy were used to analyze the wetting/dewetting process. Au-Fe_3O_4 HD nanoparticles undergo a partial dewetting procedure that can be used as a way to produce Janus particles, which is not undergone by the Pt-Fe_3O_4 HD particles. Furthermore, reduction of Fe_3O_4 to Fe was detected when experiments were performed on both silicon nitride and carbon support membranes, and the extent of reduction was more rigorous for Pt heterodimer nanoparticles. The laser heating technique was shown to be a useful and novel method to undergo such in situ heating experiments to underpin future development of functional heterodimer nanoparticles.

Data Availability

The data used to support the findings of this study are included within the article and supplementary information files.

Conflicts of Interest

The authors declare no competing interests.

Authors' Contributions

G. M. and SN.S. conducted the experiments, analyzed the results, and wrote the manuscript equally. M.M. and C.W. provided the samples and reviewed the manuscript. S.K. worked on the initial draft, and V.O. conceived the experiment and reviewed the manuscript. Garrett M. Mitchell and Shoumya Nandy Shuvo contributed equally to this work.

Acknowledgments

This work was supported by the Designing Materials to Revolutionize and Engineer our Future (DMREF) program of the National Science Foundation (CBET-1437219). This work was also supported by the Multidisciplinary University Research Initiative Program of Department of Defense Office of Naval Research (Grant Number: 108329). Part of the TEM work was carried out at Florida State University, and the TEM facility at FSU is funded and supported by the Florida State University Research Foundation, National High Magnetic Field Laboratory (NSF-DMR-0654118), and the State of Florida. Special thanks are due to Trevor Lardinois for his help in collection of the DRUV-Vis spectra.

Supplementary Materials

Supporting Movie-1 shows an in situ BF-TEM video of the Pt-Fe_3O_4 HD nanoparticles undergoing laser heating. The Pt are seen to wet on the surface of the iron oxide and subsequently undergo sintering (https://drive.google.com/file/d/1nLQg5XNDzjTTXX5we60kX1NSwzjehPEp/view?usp=sharing). Figure S1: DRUV–Vis spectra of model sample silicon nitride and amorphous carbon. *(Supplementary Materials)*

References

[1] K. Fujimoto, F. H. Ribeiro, M. Avalos-Borja, and E. Iglesia, "Structure and reactivity of PdO_x/ZrO_2Catalysts for methane oxidation at low temperatures," *Journal of Catalysis*, vol. 179, pp. 431–442, 1998.

[2] D. Andreeva, V. Idakiev, T. Tabakova, A. Andreev, and R. Giovanoli, "Low-temperature water-gas shift reaction on Auα-Fe_2O_3 catalyst," *Applied Catalysis A: General*, vol. 134, pp. 275–283, 1996.

[3] B. A. A. Silberova, G. Mul, M. Makkee, and J. A. Moulijn, "DRIFTS study of the water–gas shift reaction over Au/Fe_2O_3," *Journal of Catalysis*, vol. 243, no. 1, pp. 171–182, 2006.

[4] A. A. Herzing, C. J. Kiely, A. F. Carley, P. Landon, and G. J. Hutchings, "Identification of active gold nanoclusters on iron oxide supports for CO oxidation," *Science*, vol. 321, no. 5894, pp. 1331–1335, 2008.

[5] K. Zhao, B. Qiao, J. Wang, Y. Zhang, and T. Zhang, "A highly active and sintering-resistant Au/FeOx–hydroxyapatite catalyst for CO oxidation," *Chemical Communications*, vol. 47, no. 6, pp. 1779–1781, 2011.

[6] S. Kundu, A. Leelavathi, G. Madras, and N. Ravishankar, "Room temperature growth of ultrathin au nanowires with high areal density over large areas by in situ functionalization of substrate," *Langmuir*, vol. 30, pp. 12690–12695, 2014.

[7] F. Lin and R. Doong, "Bifunctional Au–Fe3O4Heterostructures for magnetically recyclable catalysis of nitrophenol reduction," *Journal of Physical Chemistry C*, vol. 115, no. 14, pp. 6591–6598, 2011.

[8] G. Cao, *Nanostructures and Nanomaterials: Synthesis, Properties and Applications*, World Scientific, 2004.

[9] Y. P. Xie, G. Liu, L. Yin, and H.-M. Cheng, "Crystal facet-dependent photocatalytic oxidation and reduction reactivity of monoclinic WO_3 for solar energy conversion," *Journal of Materials Chemistry*, vol. 22, no. 14, pp. 6746–6751, 2012.

[10] M. Haruta, "Size- and support-dependency in the catalysis of gold," *Catalysis Today*, vol. 36, no. 1, pp. 153–166, 1997.

[11] J. A. Farmer and C. T. Campbell, "Ceria maintains smaller metal catalyst particles by strong metal-support bonding," *Science*, vol. 329, no. 5994, pp. 933–936, 2010.

[12] Q. Fu, H. Saltsburg, and M. Flytzani-Stephanopoulos, "Active nonmetallic Au and Pt species on ceria-based water-gas shift catalysts," *Science*, vol. 301, no. 5635, pp. 935–938, 2003.

[13] Q. Fu, A. Weber, and M. Flytzani-Stephanopoulos, "Nanostructured Au–CeO_2 catalysts for low-temperature water–gas shift," *Catalysis Letters*, vol. 77, no. 1/3, pp. 87–95, 2001.

[14] M. B. Boucher, S. Goergen, N. Yi, and M. Flytzani-Stephanopoulos, "'Shape effects' in metal oxide supported nanoscale gold catalysts," *Physical Chemistry Chemical Physics*, vol. 13, 2011.

[15] I. Laoufi, M. C. Saint-Lager, R. Lazzari et al., "Size and catalytic activity of supported gold nanoparticles: an in operando study during CO oxidation," *Journal of Physical Chemistry C*, vol. 115, pp. 4673–4679, 2011.

[16] C.-H. Tu, A.-Q. Wang, M.-Y. Zheng, X.-D. Wang, and T. Zhang, "Factors influencing the catalytic activity of SBA-15-supported copper nanoparticles in CO oxidation," *Applied Catalysis A: General*, vol. 297, pp. 40–47, 2006.

[17] U. Kreibig and M. Vollmer, "Theoretical considerations," in *Optical Properties of Metal Clusters*, pp. 13–201, Springer, 1995.

[18] C. F. Bohren and D. R. Huffman, *Absorption and scattering of light by small particles*, John Wiley & Sons, 2008.

[19] A. Leelavathi, B. Mukherjee, C. Nethravathi et al., "Highly photoactive heterostructures of PbO quantum dots on TiO_2," *RSC Advances*, vol. 3, no. 43, pp. 20970–20977, 2013.

[20] D. Li and Y. Xia, "welding and patterning in a flash," *Nature Materials*, vol. 3, no. 11, pp. 753-754, 2004.

[21] B. O'regan and M. Grfitzeli, "A low-cost, high-efficiency solar cell based on dye-sensitized colloidal TiO2 films," *Nature*, vol. 353, no. 6346, pp. 737–740, 1991.

[22] Y. Tachibana, L. Vayssieres, and J. R. Durrant, "Artificial photosynthesis for solar water-splitting," *Nature Photonics*, vol. 6, 2012.

[23] A. M. Morales and C. M. Lieber, "A Laser Ablation Method for the Synthesis of Crystalline Semiconductor Nanowires," *Science*, vol. 279, no. 5348, pp. 208–211, 1998.

[24] H. Zeng, X. W. Du, S. C. Singh et al., "Nanomaterials via laser ablation/irradiation in liquid: a review," *Advanced Functional Materials*, vol. 22, pp. 1333–1353, 2012.

[25] A. H. Zewail, "4D ultrafast electron diffraction, crystallography, and microscopy," *Annual Review of Physical Chemistry*, vol. 57, pp. 65–103, 2006.

[26] R. M. van der Veen, T. J. Penfold, and A. H. Zewail, "Ultrafast core-loss spectroscopy in four-dimensional electron microscopy," *Structural dynamics*, vol. 2, no. 2, 2015.

[27] D. J. Flannigan and A. H. Zewail, "4D electron microscopy: principles and applications," *Accounts of Chemical Research*, vol. 45, pp. 1828–1839, 2012.

[28] D. Shorokhov and A. H. Zewail, "Perspective: 4D ultrafast electron microscopy—evolutions and revolutions," *The Journal of chemical physics*, vol. 144, no. 8, p. 080901, 2016.

[29] A. H. Zewail, "Four-dimensional electron microscopy," *Science*, vol. 328, no. 5975, pp. 187–193, 2010.

[30] B. Barwick and A. H. Zewail, "Photonics and plasmonics in 4D ultrafast electron microscopy," *ACS Photonics*, vol. 2, pp. 1391–1402, 2015.

[31] H. S. Park, J. S. Baskin, O.-H. Kwon, and A. H. Zewail, "Atomic-scale imaging in real and energy space developed in ultrafast electron microscopy," *Nano Letters*, vol. 7, pp. 2545–2551, 2007.

[32] H. Yu, M. Chen, P. M. Rice, S. X. Wang, R. L. White, and S. Sun, "Dumbbell-like bifunctional Au– Fe_3O_4 nanoparticles," *Nano Letters*, vol. 5, pp. 379–382, 2005.

[33] Y. Lee, M. A. Garcia, N. A. Frey Huls, and S. Sun, "Synthetic tuning of the catalytic properties of Au-Fe_3O_4 nanoparticles," *Angewandte Chemie International Edition*, vol. 122, pp. 1293–1296, 2010.

[34] H. Yin, C. Wang, H. Zhu, S. H. Overbury, S. Sun, and S. Dai, "Colloidal deposition synthesis of supported gold nanocatalysts based on Au–Fe_3O_4 dumbbell nanoparticles," *Chemical Communications*, vol. 36, pp. 4357–4359, 2008.

[35] J. Kunze, *Nitrogen and Carbon in Iron and Steel Thermodynamics*, Akademie Verlag (Akademie-Verlag, Berlin, 1990.

[36] C. W. Han, T. Choksi, C. Milligan et al., "A discovery of strong metal-support bonding in Nanoengineered Au–Fe3O4Dumbbell-like nanoparticles by in Situ transmission electron microscopy," *Nano Letters*, vol. 17, no. 8, pp. 4576–4582, 2017.

[37] C. Gatel and E. Snoeck, "Epitaxial growth of Au and Pt on Fe_3O_4 (111) surface," *Surface Science*, vol. 601, pp. 1031–1039, 2007.

[38] C. Gatel and E. Snoeck, "Comparative study of Pt, Au and Ag growth on Fe_3O_4 (001) surface," *Surface Science*, vol. 600, no. 13, pp. 2650–2662, 2006.

[39] N. E. Singh-Miller and N. Marzari, "Surface energies, work functions, and surface relaxations of low-index metallic surfaces from first principles," *Physical Review B*, vol. 80, article 235407, 2009.

[40] L. Vitos, A. V. Ruban, H. L. Skriver, and J. Kollár, "The surface energy of metals," *Surface Science*, vol. 411, pp. 186–202, 1998.

[41] W. M. Haynes, *CRC Handbook of Chemistry and Physics*, CRC press, 2014.

[42] C. Creemers, S. Helfensteyn, J. Luyten, and M. Schurmans, "Synergy between Material, Surface Science Experiments and Simulations," in *Applied Computational Materials Modeling*, pp. 109–169, Springer, US, 2007.

[43] H. Fuse, N. Koshizaki, Y. Ishikawa, and Z. Swiatkowska-Warkocka, "Determining the composite structure of Au-Fe-based submicrometre spherical particles fabricated by pulsed-laser melting in liquid," *Nanomaterials*, vol. 9, 2019.

[44] M. R. Buck, J. F. Bondi, and R. E. Schaak, "A total-synthesis framework for the construction of high-order colloidal hybrid nanoparticles," *Nature chemistry*, vol. 4, no. 1, pp. 37–44, 2012.

[45] F. Hu, H. Lin, Z. Zhang et al., "Smart liquid SERS substrates based on Fe_3O_4/Au nanoparticles with reversibly tunable enhancement factor for practical quantitative detection," *Scientific Reports*, vol. 4, no. 1, 2015.

[46] G. D. Pirngruber, P. K. Roy, and R. Prins, "The role of autoreduction and of oxygen mobility in N_2O decomposition over Fe-ZSM-5," *Journal of Catalysis*, vol. 246, no. 1, pp. 147–157, 2007.

[47] C. C. Ahn, *Transmission Electron Energy Loss Spectrometry in Materials Science and the EELS Atlas*, John Wiley & Sons, 2006.

[48] H. Tan, J. Verbeeck, A. Abakumov, and G. Van Tendeloo, "Oxidation state and chemical shift investigation in transition metal oxides by EELS," *Ultramicroscopy*, vol. 116, pp. 24–33, 2012.

[49] P. A. van Aken and B. Liebscher, "Quantification of ferrous/ferric ratios in minerals: new evaluation schemes of Fe L_{23} electron energy-loss near-edge spectra," *Physics and Chemistry of Minerals*, vol. 29, pp. 188–200, 2002.

[50] R. F. Egerton, *Electron Energy-Loss Spectroscopy in the Electron Microscope*, Springer Science & Business Media, 2011.